engineering proceedings

MDPI

Proceeding Paper

Development of an Integrated Satellite-Based Estimation Method for Water Transparency and Algal Beds in the Mekong River †

Tomonari Masuzaki [1,*], Shuta Murakami [2], Supachai Prainetr [3,*] and Ganbat Davaa [1]

[1] National Institute of Technology, Yuge College, Kamijima 794-2593, Japan
[2] Department of Computer Science and Engineering, Toyohashi University of Technology, Toyohashi 441-8580, Japan
[3] Department of Electrical Engineering, Faculty of Industrial Technology, Nakhon Phanom University, Nakhon Phanom 48000, Thailand
* Correspondence: t_masuzaki@info.yuge.ac.jp (T.M.); prainetr@npu.ac.th (S.P.); Tel.: +81-897-77-4606 (T.M.); +81-1178358 (S.P.)
† Presented at the 2nd International Conference on AI Sensors and Transducers, Kuala Lumpur, Malaysia, 29 July–3 August 2025.

Abstract

This study presents an integrated satellite-based approach for estimating water transparency and algal bed distribution in the dynamic environment of the Mekong River using satellite imagery. Recognizing that previous research has predominantly focused on marine settings, this work addresses the unique challenges inherent in riverine systems like the Mekong, where low and variable transparency demands specialized techniques. Utilizing Sentinel-2 satellite data, a system was developed that compensates for water depth effects through the Bottom Index—a metric derived from the reflective properties of the riverbed. This approach effectively minimizes the influence of water depth variability on remote sensing data and enhances the accuracy of bottom characterization. Concurrently, water transparency is estimated via a ratio-based statistical model that correlates reflectance values from two selected bands to compute the Secchi-Disk Depth. Field experiments conducted in both coastal waters demonstrated that the estimated results align with in situ observations in algal bed distribution.

Keywords: algal bed mapping; remote sensing; water transparency estimation

check for updates

Academic Editor: Sang-Seok Lee

Published: 14 October 2025

Citation: Masuzaki, T.; Murakami, S.; Prainetr, S.; Davaa, G. Development of an Integrated Satellite-Based Estimation Method for Water Transparency and Algal Beds in the Mekong River. *Eng. Proc.* **2025**, *110*, 2. https://doi.org/10.3390/engproc2025110002

Copyright: © 2025 by the authors. Licensee MDPI, Basel, Switzerland. This article is an open access article distributed under the terms and conditions of the Creative Commons Attribution (CC BY) license (https://creativecommons.org/licenses/by/4.0/).

1. Introduction

The Mekong River underpins diverse ecosystems and livelihoods across Southeast Asia but is undergoing pronounced environmental change driven by hydropower development, altered flow and sediment regimes, and climate variability [1]. Efficient, repeated, basin-scale monitoring of water transparency and algal vegetation is therefore essential. At the management interface, basin-scale information also supports evaluating the resilience of nature-based treatment systems under variable contaminant loads [2]. The Mekong River is characterized by high turbidity and strong seasonal variation in suspended sediment load, influenced by upstream hydropower dams, monsoonal flow changes, and flood–drought cycles. These drivers cause frequent low-transparency conditions, making conventional single-indicator mapping (e.g., using SDD or BI alone) prone to false positives or incomplete retrievals. By explicitly integrating SDD-derived transparency constraints into BI mapping, our workflow targets only optically suitable pixels, thereby improving reliability compared to traditional approaches.

Cloud-based geospatial platforms such as Google Earth Engine (GEE) enable the processing of petabyte-scale satellite archives, making wide-area, high-frequency aquatic assessments feasible using sensors like Sentinel-2. Recent reviews emphasize that successful inland water quality retrievals hinge on sensor choice, atmospheric correction, and tailored bio-optical modeling [3]. Furthermore, AI-driven GEE applications for water monitoring (e.g., algal bloom predictions, temporal trend detection) show the platform's growing power in environmental monitoring [4]. Beyond habitat mapping, these data streams also support ecosystem and carbon-cycle assessments; recent syntheses highlight growing use of satellite-derived clarity and productivity indicators and ecosystem-model ensembles [5,6].

In the Mekong context, recent work by Nontapon et al. employed Landsat-8 imagery validated by in situ data (2017–2023) to estimate suspended sediment concentration (SSC) using indices such as NDSSI, NSMI, and NDTI, achieving an R^2 of approximately 0.72 for NDSSI and demonstrating the feasibility of satellite-based sediment monitoring in highly turbid rivers [7]. Building upon this foundation, our study extends the application of satellite data from surface-sediment estimation to subsurface optical analysis by integrating Secchi Disk Depth (SDD) and the Bottom Index (BI) within a unified GEE workflow. This approach enhances interpretability and seeks to improve reliability by ensuring that benthic mapping is performed only in sufficiently transparent water areas, a critical improvement over single-index methods in optically complex rivers like the Mekong.

In coastal and relatively clear waters, depth-invariant/bottom-reflectance methods (BI-type) and passive multispectral bathymetry are well established [8], including integrated mapping of water quality and substrates in optically complex waters [9] and turbidity retrievals from deltaic to coastal zones [10]. Operational examples include quantitative mapping of algal and seagrass beds in Innoshima, Seto Inland Sea [11], and satellite-based transparency (Secchi disk depth, SDD) estimation off Hiroshima following the 2018 heavy-rain event [12], alongside clarity-oriented algorithm refinements [13]. However, direct transfer to highly turbid, fast-changing rivers is non-trivial; depth-invariant formulations often presume spatially uniform optics, and ratio-based transparency regressions need local calibration. We therefore link a reflectance-ratio SDD estimator with a transparency-aware Bottom Index in a single GEE workflow and apply it at Yuge Island (Japan) and along the Mekong near Nakhon Phanom (Thailand).

2. Materials and Methods

2.1. Data and Platform

In this study, we analyze water transparency and algal bed distribution using satellite imagery. Experiments were conducted at two locations: coastal waters in Japan's Seto Inland Sea (near Yuge Island) and a reach of the Mekong River in Thailand (near Nakhon Phanom). We used Sentinel-2 imagery for all analyses. Sentinel-2 carries the Multispectral Instrument (MSI), a 13-band push-broom sensor spanning the visible to short-wave infrared (443–2190 nm) with spatial resolutions of 10/20/60 m and a ~290 km swath. The Sentinel-2 mission is operated by the European Space Agency (ESA) as part of the Copernicus Program and provides freely accessible global multispectral data. All satellite scenes used in this study were obtained via the Google Earth Engine (GEE) platform. In this study we use surface reflectance from Sentinel-2. The Green–NIR pair (B3, B8) is used for Normalized Difference Water Index (NDWI)-based water masking; B3, B4, and B12 are used in the transparency (SDD) estimator; and the Bottom Index (BI) is evaluated from paired bands using shallow/deep reference samples. Table 1 summarizes the Sentinel-2 bands used in this study, including their center wavelengths and spatial resolutions.

Table 1. Sentinel-2 bands used in this study.

Band	Common Name	Center Wavelength (nm)	Spatial Resolution (m)
B3	Green	560	10
B4	Red	665	10
B8	Near-Infrared (NIR)	842	10
B12	Short-Wave Infrared (SWIR)	2190	20

Processing, compositing, and custom analysis were performed on GEE (accessed in 2025). Water detection employed the NDWI computed from bands B3 (Green) and B8 (NIR). Cloud masking used the Sentinel-2 cloud probability layer with a 20% threshold.

2.2. Transparency (Secchi Disk Depth) Estimation

Generally, methods for estimating transparency from satellite data employ either semi-theoretical approaches based on water quality parameters—such as SS (suspended solids), turbidity, Chla (chlorophyll a concentration), and CDOM (colored dissolved organic matter)—which are primary drivers of transparency, or statistical methods (see also reviews and clarity-algorithm work in aquatic optics) [13]. Related satellite algorithms have also been used to infer phytoplankton and algal bloom metrics from multispectral data [14]. In this study, we use a statistical model based on relatively simple ratio calculations, such as the commonly used Equation (1), to estimate these water quality parameters from satellite data.

$$SDD \propto \left[\frac{R_i}{R_j}\right] \tag{1}$$

Here, Secchi-Disk Depth (SDD) represents transparency and is one of the most widely used indices for estimating water clarity in aquatic environments. The Secchi Disk is a black-and-white disk lowered into the water to measure the depth at which it becomes invisible. This depth correlates with the concentration of suspended solids and other particles that affect water transparency [15]. SDD is a well-established parameter for water quality monitoring in both coastal and freshwater environments. In this study, R_i and R_j denote the reflectance values for two bands (i and j are band numbers). Sakuno et al. [12] demonstrated that bands 3 and 4 exhibit the highest correlation, and that a reliable transparency estimation formula can be obtained by offsetting the band 12 reflectance.

To operationalize the ratio-based framework in Equation (1), we adopt a simple statistical model using selected Sentinel-2 bands (Green, Red, and SWIR):

$$SDD = 2.03\frac{R_3 - R_{12}}{R_4 - R_{12}} - 1.53, \tag{2}$$

where SDD denotes Secchi-Disk Depth (transparency), and R_i are atmospherically corrected surface reflectances for band i (B3 = Green, B4 = Red, B12 = SWIR). The band combination follows prior findings that report strong correlations between such ratios and in situ transparency. Given seasonal and spatial variability in optical conditions and particulate loads in the Mekong, Equation (2) uses parameters derived from Sakuno et al.'s experiments in the Seto Inland Sea, and is treated as an initial model. The coefficients (2.03 and 1.53) in Equation (2) were originally derived from coastal calibration in the Seto Inland Sea. Preliminary testing in the Mekong indicates that these parameters yield reasonable but slightly underestimated SDD values under high turbidity. Future work will include SDD–reflectance measurements in the Mekong to locally recalibrate these coefficients for improved model transferability.

2.3. Bottom Index (BI) for Algal-Bed Mapping

To estimate algal bed distribution while accounting for water depth, we adopt the BI.

2.3.1. BI Explanation

In shallow waters, the water-leaving reflectance depends on bottom albedo, depth, and water-column attenuation. Following Lyzenga's depth-invariant theory, combining two bands in logarithmic form cancels the explicit depth term, and the slope of the resulting relation corresponds to the attenuation-coefficient ratio between the bands [8], with subsequent applications to joint mapping of substrates and water quality in optically complex waters [9].

We denote Sentinel-2 Level-2A surface reflectance of band i by R_i (bands are resampled to a common grid before any log/ratio operation), and the deep-water mean by $\overline{R_{i,deep}}$. $\overline{R_{i,deep}}$ denotes the 5 × 5-pixel mean reflectance for each band, calculated at locations selected as sufficiently deep. The BI at pixel x is

$$\mathrm{BI}(x) = \ln\left(R_i(x) - \overline{R_{i,deep}}\right) - k_{ij}\ln\left(R_j(x) - \overline{R_{i,deep}}\right), \tag{3}$$

where k_{ij} is the inter-band attenuation-coefficient ratio and i, j denote Sentinel-2 band indices (B3 = Green; B4 = Red; B12 = SWIR). Within an empirically set range, higher BI values indicate vegetation-like bottoms, whereas lower values suggest sand or non-vegetated substrate. In practice we evaluate BI only within NDWI-detected water.

2.3.2. Deriving the Attenuation-Coefficient Ratio k_{ij}

To derive the inter-band attenuation-coefficient ratio k_{ij}, we employ a shallow and nearby deep-water contrast approach and perform the regression in logarithmic space; that is, we take the natural logarithms of the band-wise contrasts and estimate k_{ij} as the slope of the linear relationship between $\ln \Delta R_i$ and $\ln \Delta R_j$ as in coastal applications by Katsube et al. The procedure for deriving k_{ij} is as follows.

1. Shallow-sand sampling. Identify 20 locations that are shallow and sandy; extract 3 × 3-pixel means for each band and compute their mean values.
2. Deep-water sampling. Identify locations that are sufficiently deep; extract 5 × 5-pixel means for each band.
3. Band-wise contrasts. For each corresponding band, compute the contrast as $\Delta R_i = \overline{R_{i,shallow}} - \overline{R_{i,deep}}$.
4. Log-log regression. Regress $\ln \Delta R_i$ on $\ln \Delta R_j$; the slope of this linear relationship is the attenuation coefficient ratio k_{ij}.

With k_{ij} thus obtained, substitute it into Equation (3) to evaluate the BI and infer bottom type. Practical notes.

2.4. Proposed Work Flow: Transparency-Aware Bottom Index Mapping

This section presents a complete, reproducible workflow to map algal bed distribution while accounting for water depth and water-column variability. The method integrates a ratio-based transparency (SDD) estimator (Equation (2)) with a depth-invariant BI formulation (Equation (3)) under a single processing pipeline on GEE. The SDD map is used both to stabilize the depth-correction parameters and to constrain BI evaluation to optically plausible water, enabling robust application in turbid, seasonally variable riverine settings.

1. Input and pre-processing. Sentinel-2 scenes are acquired and filtered for clouds. All bands required for SDD and BI are resampled to a common spatial resolution, and computations are confined to NDWI-detected water to exclude land and mixed pixels.

2. Transparency mapping. A simple ratio-based statistical model using selected bands (Green, Red, SWIR) produces a wall-to-wall SDD map over water consistent with prior clarity-focused satellite approaches [13].
3. Construction and pairing of reference sets. Shallow sandy references (20 locations using 3 × 3-pixel means) and nearby deep-water references (using 5 × 5-pixel means) are identified for each scene. Each shallow reference is paired with deep water exhibiting similar SDD to form stable shallow–deep contrasts under variable turbidity.
4. Derivation of the attenuation-coefficient ratio. For each band i, the contrast $\Delta R_i = \overline{R_{i,shallow}} - \overline{R_{i,deep}}$ is computed. A log-log regression of $\ln \Delta R_i$ on $\ln \Delta R_j$ yields the slope k_{ij}, interpreted as the inter band attenuation-coefficient ratio.
5. Bottom Index mapping. Using the estimated k_{ij} and deep-water means, BI is evaluated for water pixels.
6. Transparency-aware Masking. Constrain BI to pixels that fall in the 'Red' SDD color bin, which—under our visualization scheme (0.5–5.5 m split into five equal-width bins with upper-end clamping)—corresponds to SDD $\gtrsim$ 4.5 m (values $\geq$ 5.5 m are rounded/clamped into the red bin). This mask is identical to the red areas shown in the SDD layer.
7. Visualization. Generate a BI color map to show the algal bed distribution.

To increase the reliability of the results, we compute BI only within high-transparency water identified by the 'Red' SDD color bin under our visualization scheme (0.5–5.5 m split into five equal-width bins with upper-end clamping), i.e., SDD $\gtrsim$ 4.5 m (values $\geq$ 5.5 m are also clamped into red). Restricting BI to these pixels minimizes water-column attenuation and turbidity-driven variability, yielding more stable bottom-contrast estimates than running BI over all water. Shallow–deep pairing and the attenuation ratio $\boldsymbol{k}_{23}$ are still estimated locally to reflect scene-specific optics, and the full sequence—NDWI masking SDD mapping $\boldsymbol{k}_{23}$ estimation → BI evaluation → red-bin masking—is implemented end-to-end on GEE, ensuring consistent and reproducible reprocessing across sites and dates.

3. Results and Discussion

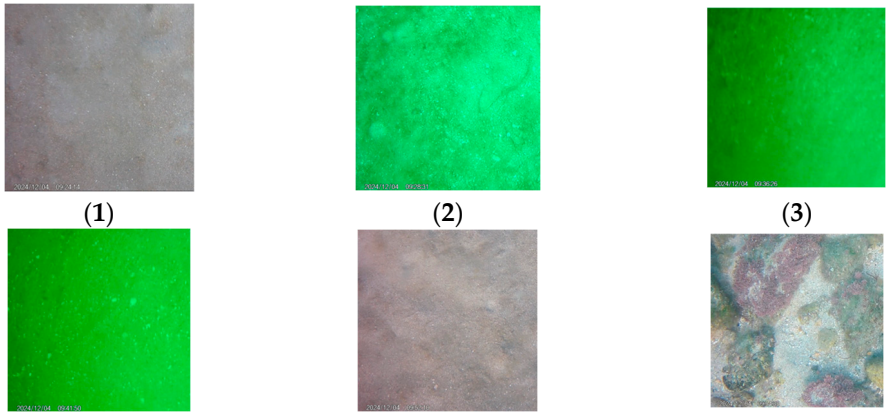
3.1. Coastal Validation near Yuge Island (Japan)

Comparison of the estimation results of our method with actual seabed conditions confirms the validity of the proposed method. This experiment was conducted on 4 December 2024. The closest satellite imagery on the day of the experiment was taken on 8 December, and the imagery was used to estimate the algal beds. The results of the estimation and mapping of the results are shown in Figure 1. Figure 1 (1) shows the SDD estimation results. In the figure, red indicates higher transparency, while blue indicates lower transparency. In Figure 1 (2), the closer the mapping color is to red, the more likely it is that algal beds are present. For points 1-6 shown in Figure 1 (1), the seabed was photographed and compared with the estimated results. The results of the imaging of each point on the seabed are shown in Figure 2. Comparisons between the estimated and actual results are shown in Table 2. In site 2, the estimated SDD reached an abnormally high value of 30,917,450.48 m with BI = 1.70, clearly indicating a noise-induced artifact. Site 3 also showed a high BI (1.74) and SDD (5.42 m) despite a sandy substrate, implying misclassification due to local reflectance anomalies. Conversely, site 6, which was an actual algal bed, yielded SDD = 5.27 m and BI = 0.08, falling below the BI threshold and thus being missed. These discrepancies suggest that excessive reflectance or atmospheric contamination may cause overestimation of BI, while low-contrast seabed reflectance can suppress BI values.



(**1**) (**2**)

Figure 1. Estimated results of SDD and algal beds near Yuge Island. (**1**) The estimated SDD results and indicates the survey locations on the seafloor (1)–(6); (**2**) the estimated results for algal beds. The white boxes indicate survey locations. The threshold for algal-bed classification corresponded to BI $\approx$ 1.0 or higher and SDD $\geq$ 4.5 m (red range).



(**1**) (**2**) (**3**)

(**4**) (**5**) (**6**)

Figure 2. Photography results of the seabed survey. The points at which the seabed was photographed are shown in (**1**)–(**6**).

Table 2. Seabed Survey Results. Estimation results red as algal beds and all other results as sandy beds. Photography results are visually determined to be algal beds or sandy beds.

Location	Estimated Results	Photography Results
(1)	Sandy bed	Sandy bed
(2)	Algal bed	Sandy bed
(3)	Algal bed	Sandy bed
(4)	Sandy bed	Sandy bed
(5)	Sandy bed	Sandy bed
(6)	Sandy bed	Algal bed

The four-day offset between the field survey (4 December 2024) and Sentinel-2 imagery (8 December 2024) may have introduced small discrepancies in SDD due to tidal and atmospheric variability. Nevertheless, spatial correspondence between measured and mapped transparency was consistent, suggesting minimal impact.

3.2. Mekong River near Nakhon Phanom (Thailand)

Using the clicked center on the Mekong River, we computed annual time series of SDD and BI as 3 $\times$ 3-pixel neighborhood means (10 m for BI, 20 m for SDD). The monthly statistics derived from all valid Sentinel-2 scenes per month are summarized in Figure 3. Because cloud cover and data quality filters (NDWI > 0 and cloud probability < 20%) yielded different numbers of valid scenes across months, we report monthly means based on the available observations rather than fixed sample sizes.

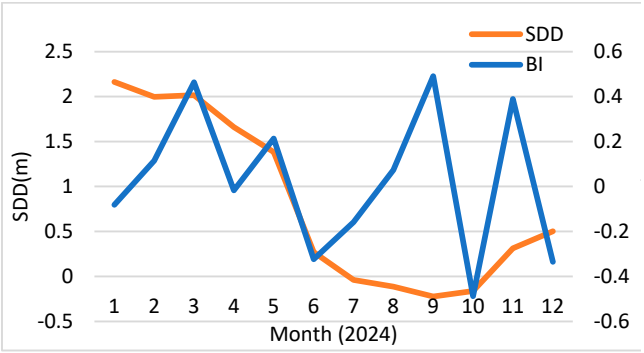


Figure 3. Monthly means of SDD (20 m) and BI (3 × 3-pixel neighborhood at 10 m) at the Mekong site (17.2760° N, 104.8010° E) for 2024; bars show the number of valid scenes.

Figure 4 illustrates February as a representative low-transparency month: SDD is consistently small, and the transparency mask therefore limits BI evaluation to very few water pixels. As a result, the mapped algal bed candidates are sparse or absent in February.



(**1**) (**2**)

Figure 4. February example at the Mekong site: (**1**) SDD map; (**2**) BI results restricted to the high-transparency (red-bin) mask. The SDD color scale covers 0.5 – 5.5 m and the BI scale ranges from −2 to +2.

Across the year, SDD varies in phase with Thailand's rainy/dry seasons, but typically remains below ~3 m at the study point. Under such conditions the optical water column is not sufficiently clear to support robust bottom-reflectance retrievals. Consequently, BI values at this site generally stay below empirically useful ranges for algal bed detection, and no month shows a sustained period indicative of likely algal bed presence.

Because our transparency model (Equation (2)) was parameterized from Seto Inland Sea experiments and not locally recalibrated, the SDD estimates—and thus the BI masking—should be regarded as initial. Field measurements in the Mekong are needed both to recalibrate Equation (2) and to validate BI-based habitat mapping; until then, the BI results should be treated as low-confidence under the prevailing low-transparency conditions.

3.3. Discussion

Our results demonstrate that transparency-aware BI is feasible on GEE but its applicability is limited when SDD < 3 m. Future work should include in situ calibration of Equation (2) parameters for Mekong waters to improve SDD accuracy. Testing alternative band pairs (e.g., B2–B4, B3–B8) may enhance robustness under high-turbidity conditions. Compared with single-indicator approaches, our method significantly reduces false positives by gating BI to high-transparency pixels, a strategy not widely applied in riverine algal-bed mapping.

4. Conclusions

We presented a GEE-based Sentinel-2 workflow linking SDD and a transparency-aware BI. Coastal experiments validated the feasibility of the proposed workflow, while its

application to the Mekong demonstrated that persistently low SDD substantially constrains the reliable estimation and mapping of algal beds.

Future research will focus on collecting in situ SDD–reflectance pairs in the Mekong to calibrate Equation (2) and conducting additional seabed surveys at Yuge Island to improve validation coverage.

Author Contributions: Conceptualization, T.M., S.M. and G.D.; Methodology, T.M., S.M. and G.D.; Software, T.M., S.M. and G.D.; Formal Analysis, T.M.; Investigation, T.M., S.M. and G.D.; Writing—Original Draft, T.M.; Writing—Review and Editing, S.M., G.D., S.P. and T.M.; Supervision, S.M., G.D., S.P. and T.M. All authors have read and agreed to the published version of the manuscript.

Funding: This research was made possible in part by the support of the Japan Student Services Organization (JASSO), which enabled travel to Thailand for field surveys and collaboration.

Institutional Review Board Statement: Not applicable.

Informed Consent Statement: Not applicable.

Data Availability Statement: The satellite data used in this study are publicly available from the Copernicus Open Access Hub and can also be accessed through Google Earth Engine (GEE) under the dataset ID COPERNICUS/S2_SR_HARMONIZED. Field survey data collected at Yuge Island (Japan) and the Mekong River (Thailand) are stored securely by the corresponding author and are available on reasonable request due to research collaboration agreements and local data-sharing restrictions. No other new data were created or analyzed in this study.

Acknowledgments: We thank the students and colleagues at National Institute of Technology (KOSEN), Yuge College and Nakhon Phanom University for their support.

Conflicts of Interest: The authors declare no conflicts of interest.

References

1. Mekong River Commission. *State of the Basin Reports 2023*; MRC Secretariat: Vientiane, Laos, 2023.
2. Raj, A.V.; Jamwal, P. Assessing resilience of natural treatment system to variable contaminant loads in an urbanizing catchment. *J. Water Process Eng.* **2024**, *58*, 104774. [CrossRef]
3. Ansari, M.; Knudby, A.; Amani, M.; Sawada, M. Retrieving Inland Water Quality Parameters via Satellite Remote Sensing: Sensor Evaluation, Atmospheric Correction, and Machine Learning Approaches. *Remote Sens.* **2025**, *17*, 1734. [CrossRef]
4. Jahangeer, J.; Pranjay, J.; Aditya, K.; Zhenghong, T. A review of AI-driven Google Earth Engine applications in surface water monitoring, assessment, and management. *Discov. Geosci.* **2025**, *3*, 140. [CrossRef] [PubMed]
5. Gao, Y.; Jia, J.; Lu, Y.; Yang, T.; Lyu, S.; Shi, K.; Zhou, F.; Yu, G. Determining dominating control mechanisms of inland water carbon cycling processes and associated gross primary productivity on regional and global scales. *Earth-Sci. Rev.* **2021**, *213*, 103497. [CrossRef]
6. Neumann, A.; Fernando, Y.; Saber, A.; Arhonditsis, G.B. Toward the development of an ecosystem model ensemble to support adaptive management in Lake Ontario. *Environ. Rev.* **2024**, *32*, 231–262. [CrossRef]
7. Nontapon, J.; Srihanu, N.; Auttarapong, D.; Hasita, S.; Ratanachotinun, J.; Bhurtyal, U.; Kaewplang, S. Assessment of Suspended Sediment Concentration in the Mekong River Using Landsat-8 Data. *Eng. Access* **2025**, *11*, 233–242.
8. Lyzenga, D.R. Passive remote sensing techniques for mapping water depth and bottom features. *Appl. Opt.* **1978**, *17*, 379–383. [CrossRef] [PubMed]
9. Phinn, S.R.; Dekker, A.G.; Brando, V.E.; Roelfsema, C.M. Mapping water quality and substrate cover in optically complex coastal and reef waters: An integrated approach. *Mar. Pollut. Bull.* **2005**, *51*, 459–469. [CrossRef] [PubMed]
10. Güttler, F.N.; Niculescu, S.; Gohin, F. Turbidity retrieval and monitoring of Danube Delta waters using multi-sensor optical remote sensing data: An integrated view from the delta plain lakes to the western–northwestern Black Sea coastal zone. *Remote Sens. Environ.* **2013**, *132*, 86–101. [CrossRef]
11. Katsube, Y.; Sekita, R. Quantitative Analysis for Seaweed and Seagrass Beds Using Satellite Remote Sensing Data in Coastal Waters of Innoshima. In *Annual Report of the Faculty of Life Science and Biotechnology*; Fukuyama University: Fukuyama, Japan, 2021; Volume 31, pp. 1–15.
12. Sakuno, Y. Transparency distribution characteristics off Hiroshima before and after the 2018 Western Japan heavy rain, based on field surveys and satellite data. *Jpn. Soc. Civ. Eng. B2 (Coast. Eng.)* **2019**, *75*, I_1045–I_1050. (In Japanese)

13. Xu, M.; Barnes, B.B.; Hu, C.; Carlson, P.R.; Yarbro, L.A. Water clarity monitoring in complex coastal environments: Leveraging seagrass light requirement toward more functional satellite ocean color algorithms. *Remote Sens. Environ.* **2023**, *286*, 113418. [CrossRef]
14. Karydis, M.; Kitsiou, D. Marine water quality monitoring: A review. *Mar. Pollut. Bull.* **2013**, *77*, 23–36. [CrossRef] [PubMed]
15. Kulshreshtha, A.; Shanmugam, P. Estimation of Secchi Transparency in Turbid Coastal Waters. *Aquat. Procedia* **2015**, *4*, 1114–1118. [CrossRef]

Disclaimer/Publisher's Note: The statements, opinions and data contained in all publications are solely those of the individual author(s) and contributor(s) and not of MDPI and/or the editor(s). MDPI and/or the editor(s) disclaim responsibility for any injury to people or property resulting from any ideas, methods, instructions or products referred to in the content.